Korean J. of Chem. Eng., **12**(1), 80-87 (1995)

MODELING OF TRANSIENT HETEROGENEOUS TWO-DIMENSIONAL CATALYTIC PACKED BED REACTOR

Jung-Hwan Park

Department of Industrial Safety Engineering, Inchon University, Inchon, Korea
(Received 18 March 1994 • accepted 1 August 1994)

Abstract—A two-dimensional transient catalytic packed bed model, incorporating all transport parameters and resistances, along with boundary conditions based on a catalytic single pellet has been developed. Thermal conduction through the solid phase is included in the model. The overall steady state reactor performances of packed bed reactor using a model proposed in this study are compared with those from different models which are often used for a packed bed reactor. The model presented is very useful in the presence of internal temperature and concentration gradients in the catalyst pellets. The dynamic behavior in feed temperature change is examined during ethane hydrogenolysis. A transient thermal runaway is observed by feed temperature decrease. The sensitivities of the computation to each physical parameter and the effects of some simplifying assumptions in the model are also analyzed. The magnitude and position of hot spot in catalytic packed bed reactor are relatively sensitive to thermal parameters and characteristic parameters of a catalyst pellet.

Key words: Packed Reactor, Discrete-Pellet Model, Transient Thermal Runaway, Sensitivity

INTRODUCTION

General mathematical models of a packed bed reactor may be in principle necessary to include all relevant transport phenomena in order to adequately represent a system. Comprehensive transient mathematical models are usually complex due to introduction of both intraparticle and interface concentration and temperature gradients, and of the heat and mass dispersions in a packed bed reactor. This inclusion makes a reactor model very complicated and needs much computational efforts. A good review of various models of fixed bed reactor can be founded in the literature [1]. When a two dimensional heterogeneous model is used, the conservation equations for mass and energy are written separately for the fluid and catalyst phases in both axial and radial directions of the reactor. DeWasch and Froment [2] introduced the need to separately specify the fluid-wall and solid-wall heat transfer for the energy conservation equation. A heterogeneous model allows for intraparticle resistance to mass and heat within the catalyst particles, in addition to external resistance. For a catalytic packed bed, unfortunately, there is no widely accepted relationship between the pellet and continuous solid phase for the energy balance. A comparative performance of several models using lumped and individual thermal parameters has been analyzed by Pereira Duarte et al. [3]. In computation of model equations, some authors ignore intraparticle gradients [4], or use the effectiveness factor for a first order reaction in an isothermal pellet [5]. Some studies have shown that the assumption of symmetric concentration and temperature profiles provides a good estimate of internal effectiveness, even in the presence of steep reactor gradients [6-8]. Cale [9] has discussed experimental results, obtained using Nickel Crystallite Thermometry, which show that the average temperatures of Ni crystallite are very close to those of the catalyst support during ethane hydrogenolysis. There however may still be pellet scale intraparticle temperature and concentration gradients.

Although significant progress has been made in the mathematical modeling of packed bed reactors over the last decade, there are only a limited number of studies concerned with unsteady state simulations [10-13]. Fewer studies have been published which account for both axial and radial dispersions as well as intraparticle and interface gradients [4, 14-15]. Even for steady state simulation, earlier models were generally simplified substantially because of computational complexity of the modeled system. However, the important thing to be borne in chemical engineering mind is to establish the model of as realistic physical bases as possible, while ensuring that all transport phenomena in a reactor are included. Current mathematical models thus favor more physical bases. Moreover, with the advent of large computing availability, a computational complexity of the model is no longer drawback of the simulation. Feick and Quon [16] have developed an improved model which includes many important transport resistances. Their model was solved using a finite difference technique that required up to 90 min computing time. Gatica et al. [15] have also put forward a detailed unsteady state two phase model based on a single particle, which required 15 min computational time by the use of orthogonal collocation numerical method. Windes et al. [14] have dealt with quasi-steady state model. They showed that both heterogeneous and pseudo-homogeneous models can give good agreement with experimental data. All of the above models assume that heat is transferred only through the flowing medium.

In this work, more general reactor models incorporated all physical and chemical transport processes are studied. The use of discrete-pellet model based on a single pellet is well warranted when the internal concentration and temperature gradients dominate the overall behavior of a fixed bed reactor. The purposes of this work are to demonstrate a detailed heterogeneous model based on a single particle, to interpret the results from a family of reactor model, to analyze the parametric sensitivity as suggested in the literature [17], and to predict effects of the operating

conditions using transient simulations. This scope is limited to the case of ethane hydrogenolysis under typical laboratory operation conditions of relatively low Reynolds numbers.

DESCRIPTION OF MODEL DEVELOPMENT

A discrete-pellet model is used to simulate a non-adiabatic, two-dimensional, heterogeneous catalytic reactor. Considering the radial thermal transport parameters for the fluid and solid phases separately [2], the boundary conditions of the energy balance in the solid phase should not be limited to a single particle, as is generally done. There are several possible descriptions for the catalyst particles. The heat conduction in the bed can be split into solid and fluid phase contributions. For the solid phase, consider the energy transport by both axial and radial conduction through the particles as well as by the convection transferred between fluid and pellets.

In developing the model, the following major considerations and assumptions are made:

1. Interface and intraparticle gradients in temperature and concentration are considered.
2. The solid is a pseudo-continuous phase for energy transport.
3. Spherical pellets are uniform and identical.
4. Physical properties of the catalyst particles depend on local bed conditions, but not depend on local pellet position.
5. The fluid velocity and porosity are allowed to vary with radial position.
6. Gas velocity variations arising from temperature and pressure changes are considered.
7. All physical properties of the reaction mixture are permitted to vary with bed position, as dictated by local conditions.
8. The variations of transport parameter arising from temperature and pressure changes are permitted to vary with bed position.
9. There is no radiant energy transport.

The transient continuity and energy equations representing these model simulations are written in dimensionless form as:

For external fluid phase

Mass balance:

$$\frac{\partial c_i}{\partial \tau} = -\frac{\partial (u c_i)}{\partial z} + \frac{1}{Pe_{am}}\frac{\partial}{\partial z}\left(D_{az}\frac{\partial c_i}{\partial z}\right) + \frac{1}{Pe_{rm}}\frac{1}{r}\frac{\partial}{\partial r}\left(D_{rr}\, r \frac{\partial c_i}{\partial r}\right) - \alpha_m (c_i - c_{pi}^{s}) \tag{1}$$

Energy balance:

$$\frac{\partial T}{\partial \tau} = -u\frac{\partial T}{\partial z} + \frac{1}{Pe_{ah}}\frac{\partial}{\partial z}\left(k_{az}\frac{\partial T}{\partial z}\right) + \frac{1}{Pe_{rh}}\frac{1}{r}\frac{\partial}{\partial r}\left(k_{rr}\, r \frac{\partial T}{\partial r}\right) - \alpha_h (T - T_p^{s}) \tag{2}$$

$$\text{at } \tau = 0,\ c_i = 1,\ T = 1 \tag{3}$$

$$\text{at } z = 0,\ \frac{\partial c_i}{\partial z} = \varepsilon_b\, Pe_{am}(c_i - 1),\ \frac{\partial T}{\partial z} = \varepsilon_b\, Pe_{ah}(T - 1) \tag{4a}$$

$$\text{at } z = 1,\ \frac{\partial c_i}{\partial z} = 0,\ \frac{\partial T}{\partial z} = 0 \tag{4b}$$

$$\text{at } r = 0,\ \frac{\partial c_i}{\partial r} = 0,\ \frac{\partial T}{\partial r} = 0 \tag{5a}$$

$$\text{at } r = 1,\ \frac{\partial c_i}{\partial r} = 0,\ \frac{\partial T}{\partial r} = Bi_w(T_a - T) \tag{5b}$$

For the pellets

$$\text{Mass balance: } \frac{\partial c_{pi}}{\partial \tau} = \frac{1}{Pe_{pm}}\frac{1}{\xi^2}\frac{\partial}{\partial \xi}\left(\xi^2 \frac{\partial c_{pi}}{\partial \xi}\right) - \gamma_m \Phi(c_p,\ T_p) \tag{6}$$

$$\text{Energy balance: } \frac{\partial T_p}{\partial \tau} = \frac{1}{Pe_{ph}}\frac{1}{\xi^2}\frac{\partial}{\partial \xi}\left(\xi^2 \frac{\partial T_p}{\partial \xi}\right) + \gamma_h \Phi(c_p,\ T_p) \tag{7}$$

$$\text{at } \tau = 0,\ c_{pi} = 1,\ T_p = 1 \tag{8}$$

$$\text{at } \xi = 0,\ \left.\begin{matrix} 0 \le z \le 1 \\ 0 \le r \le 1 \end{matrix}\right\},\ \frac{\partial c_{pi}}{\partial \xi} = 0,\ \frac{\partial T_p}{\partial \xi} = 0 \tag{9a}$$

$$\text{at } \xi = 1,\ \left.\begin{matrix} 0 \le z \le 1 \\ 0 \le r \le 1 \end{matrix}\right\},\ \frac{\partial c_{pi}}{\partial \xi} = Bi_m(c_i - c_{pi}^{s}) \tag{9b}$$

$$\text{at } \xi = 1,\ \left.\begin{matrix} 0 < z < 1 \\ 0 < r < 1 \end{matrix}\right\},\ \frac{\partial T_p}{\partial \xi} = Bi_h(T - T_p^{s}) + \beta\frac{\partial^2 \bar{T}_p}{\partial z^2} + \beta'\frac{\partial}{\partial r}\left(r\frac{\partial \bar{T}_p}{\partial r}\right) \tag{10a}$$

$$\text{at } \xi = 1,\ \left.\begin{matrix} z = 0,\ z = 1 \\ 0 < r < 1 \end{matrix}\right\},\ \frac{\partial T_p}{\partial \xi} = Bi_h(T - T_p^{s}) \tag{10b}$$

$$\text{at } \xi = 1,\ \left.\begin{matrix} 0 < z < 1 \\ r = 1 \end{matrix}\right\},\ \frac{\partial^2 \bar{T}_p}{\partial r} = Bi_{as}(T_a - \bar{T}_p) \tag{10c}$$

$$\text{where } \bar{T}_p = \int_V T_{p,jk}(\xi)\,dV \Big/ \int_V dV = 3\int_0^1 T_{p,jk}(\xi)\xi^2 d\xi \tag{10d}$$

where subscript i denotes the reactant species. A mass balance is written for each species. Detailed descriptions for each dimensionless parameter are given in the Nomenclature. For brevity, the differential equation for pressure is not listed, but it is included in the model and accounted for variations in temperature and density. The axial fluid phase boundary Equation 4a has been extensively discussed in the literature [18-21], and is widely used. The boundary Eq. (10a), for the single pellet problem, includes heat transfer with convection and dispersions in the solid phase, where $\bar{T}_p$ is the pellet average temperature, as dictated by local bed position. If the dispersion terms are omitted in Eq. (10a), it gives a simple single pellet boundary condition like that for mass. Eq. (10c) is written, as early indicated, in order to account for existence of heat transfer located at the solid-tube wall. Therefore, the use of boundary conditions developed here are feasible to overcome disadvantage of conventional single pellet boundary equations.

NUMERICAL SOLUTION

The simultaneous solution of this set of nonlinear partial differential equations is considered to be a formidable challenge. Orthogonal collocation method (OCM) is used to solve the set of transient equations. This approach is very attractive in terms of the required computational effort and accuracy [22-26]. The spatial derivative terms can be removed by the use of OCM, such that the governing equations are reduced to a set of first-order ordinary differential equations, and that the boundary equations to a set of linear algebraic equations.

After transforming Eqs. (1)-(2) and (6)-(7) at the jth, kth, and *l*th collocation points for axial, radial, and pellet radial directions, respectively, the resulting equations are:

$$\frac{\partial c_{i,jk}}{\partial \tau} = -\left(u_{jk}\sum_{n=1}^{M+2} A^z_{jn}c_{i,nk} + c_{i,jk}\sum_{n=1}^{M+2} A^z_{jn}u_{nk}\right) + \frac{1}{Pe_{am\,i,jk}}\left(\sum_{n=1}^{M+2} A^z_{jn}D_{ai,nk}\sum_{n=1}^{M+2} A^z_{jn}c_{i,nk} + D_{ai,jk}\sum_{n=1}^{M+2} B^z_{jn}c_{i,nk}\right) + \frac{1}{Pe_{rm\,i,jk}}\left(\sum_{n=1}^{L+1} A^r_{kn}D_{ri,jn}\sum_{n=1}^{L+1} A^r_{kn}c_{i,jn} + D_{ri,jk}\sum_{n=1}^{L+1} B^r_{kn}c_{i,jn}\right) - \alpha_m(c_{i,jk} - c_{pi,jk,N+1}) \quad (1')$$

$$\frac{\partial T_{jk}}{\partial \tau} = -\left(u_{jk}\sum_{n=1}^{M+2} A^z_{jn}T_{nj}\right) + \frac{1}{Pe_{ah,jk}}\left(\sum_{n=1}^{M+2} A^z_{jn}k_{fa,nk}\sum_{n=1}^{M+2} A^z_{jn}T_{nk} + k_{fa,jk}\sum_{n=1}^{M+2} B^z_{jn}T_{nk}\right) + \frac{1}{Pe_{rh,jk}}\left(\sum_{n=1}^{L+1} A^r_{kn}k_{fr,jn}\sum_{n=1}^{L+1} A^r_{kn}T_{jn} + k_{fr,jk}\sum_{n=1}^{L+1} B^r_{kn}T_{jn}\right) - \alpha_h(T_{jk} - T_{p,jk,N+1}) \quad (2')$$

$$\frac{\partial c_{pi,jkl}}{\partial \tau} = \frac{1}{Pe_{pm\,i,jkl}}\sum_{n=1}^{N+1} B^\xi_{ln}c_{pi,jkn} - \gamma_m\phi(c_{p,jkl},\ T_{p,jkl}) \quad (6')$$

$$\frac{\partial T_{p,jkl}}{\partial \tau} = \frac{1}{Pe_{ph,jkl}}\sum_{n=1}^{N+1} B^\xi_{ln}T_{p,jkn} + \gamma_h\phi(c_{p,jkl},\ T_{p,jkl}) \quad (7')$$

The Eqs. (4a)-(5b) and (9a)-(10c) for the boundary conditions are transformed as:

$$\sum_{n=1}^{M+2} A^z_{ln}c_{i,nk} = \varepsilon_b\ Pe_{ami,1k}(c_{i,1k} - 1),\quad \sum_{n=1}^{M+2} A^z_{ln}T_{nk} = \varepsilon_b\ Pe_{ah,1k}(T_{1k} - 1) \quad (4a')$$

$$\sum_{n=1}^{M+2} A^z_{M-2,n}c_{i,nk} = 0,\quad \sum_{n=1}^{M+2} A^z_{M+2,n}T_{nk} = 0 \quad (4b')$$

$$\sum_{n=1}^{L+1} A^r_{L+1,n}c_{i,jn} = 0,\quad \sum_{n=1}^{L+1} A^r_{L-1,n}T_{jn} = Bi_{wf,j,L+1}(T_{w,j,L+1} - T_{j,L+1}) \quad (5b')$$

$$\sum_{n=1}^{N-1} A^\xi_{N-1,n}c_{pi,jkn} = Bi_{mi,jk}(c_{i,jk} - c_{pi,jk,N+1}) \quad (9b')$$

$$\sum_{n=1}^{N+1} A^\xi_{N-1,n}T_{p,jkn} = Bi_{h,jk}(T_{jk} - T_{p,jk,N+1}) + \beta\sum_{n=1}^{M+2} B^z_{jn}\bar{T}_{p,nk} + \beta'\sum_{n=1}^{L+1} B^r_{kn}\bar{T}_{p,jn} \quad (10a')$$

$$\sum_{n=1}^{N-1} A^\xi_{N+1,n}T_{p,jkn} = Bi_{h,jk}(T_{jk} - T_{p,jk,N+1}) \quad (10b')$$

$$\sum_{n=1}^{L+1} A^r_{L+1,n}\bar{T}_{p,jn} = Bi_{ws,jk}(T_{w,jk} - \bar{T}_{p,jk}) \quad (10c')$$

$$\text{where } \bar{T}_{p,jk} = \sum_{n=1}^{N+1} W_n T_{p,jkn} \quad (10d')$$

where $c_{jk} = c(z_j, r_k)$, and $c_{p,jkl} = c_p(z_j, r_k, \xi)$, and a similar expression is used for the temperature. The matrices A and B, the collocation points, and the quadrature weights W are obtained by the algorithm demonstrated by elsewhere [25-26]. Note that the boundary conditions at $r=0$ and $\xi=0$ are not described because the symmetry condition is already built into the trial function, and those ones are satisfied by the trial polynomial function. The above nonlinear coupled ordinary differential equations are integrated in time using the IMSL subroutine DIVPAG based on Gear method [27].

SIMULATION OF A PACKED BED REACTOR

The transport parameters need to be estimated. The numerical values of many parameters vary with the empirical correlation, experimental data source, the chosen mathematical model, or estimation of physical properties. The fluid physical properties were determined using the methods suggested by Reid et al. [28]. Intraparticle effective diffusivities were estimated as proposed by Satterfield [29]. The source for other parameter estimation methods used is listed in Table 1 and elsewhere [30-43]. Typical values of the major parameters utilized in the computation are summarized in Table 2, in which units are based on centimeter, gram, and second.

Table 1. Physical parameter estimation sources

Physical parameter	Source
Energy dispersion coefficient	31-33
Fluid-solid heat transfer coefficient	34, 35
Fluid-wall heat transfer coefficient	36
Solid-wall heat transfer coefficient	37
Thermal conductivity of the solid	38
Mass dispersion coefficient	39
Pressure drop	40
Velocity profile	41
Porosity profile	42, 43

Table 2. Simulation conditions

Operating conditions	
Inlet feed temperature	520 K
Reactor wall temperature	520 K
Reactor pressure	1 atm
Inlet superficial velocity	31.5 cm/s
Reactor length	8 cm
Reactor diameter	1 cm
Feed mole fractions	
Ethane	0.23
Hydrogen	0.37
Helium	0.4
Other operating conditions	
Catalyst diameter	0.2 cm
Bed voidage	0.43
Pellet voidage	0.5

The simulation of the system is carried out for ethane hydrogenolysis reaction

$$C_2H_6 + H_2 \rightarrow 2CH_4. \quad (11)$$

The rate expression used in this work is:

$$\Re = 7\times10^7\ \exp(-20400/T)\ C_{C_2H_6}/C^2_{H_2}. \quad (12)$$

The kinetic numerical values are obtained in the literature [30].

RESULTS AND DISCUSSION

The simulation results using the modified discrete-pellet model (MDPM) proposed in the present study is compared with those using a family of packed bed model; i.e., the conventional discrete-pellet model (CDPM) and the continuum solid phase model (CSPM). The latter two models have commonly been used for a packed bed reactor modeling [1]. As mentioned early, the major difference between the MDPM and the CDPM is that the MDPM involves both convective and dispersion heat transfer terms for the boundary conditions at the pellet surface, as dictated in Eq.

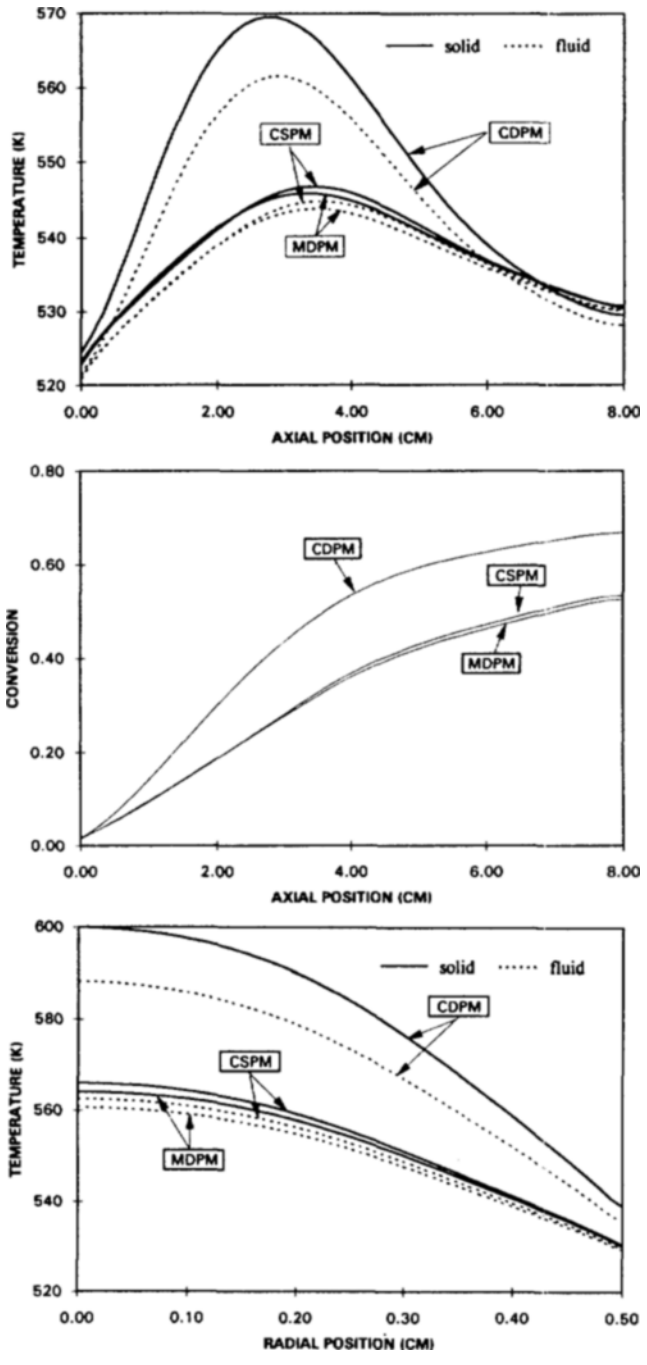

Fig. 1. Comparison of model predictions at steady state.
A. Cross-sectional average temperature profiles as functions of axial position, B. Cross-sectional average conversion profiles as functions of axial position, C. Radial temperature profiles at the hot spot.

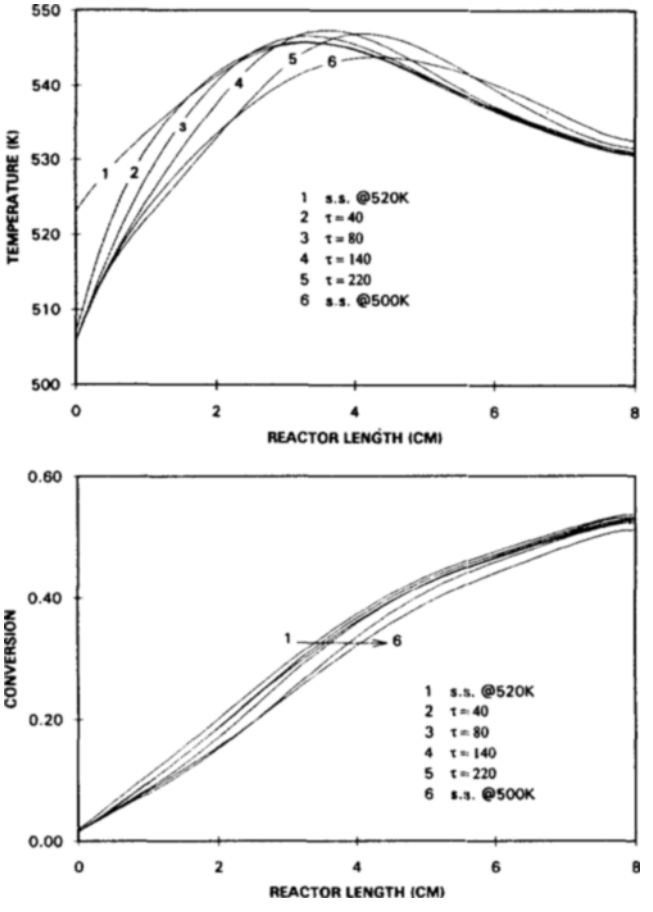

Fig. 2. Response to a step change in feed temperature from 520 K to 500 K using the MDPM.
A. Cross-sectional average solid temperature profiles as functions of reactor length, B. Ethane conversion profiles as functions of reactor length.

(10a), whereas the CDPM contains only the convection terms. In addition, the MDPM allows for the heat transfer between the solid and reactor wall, which is proposed by DeWasch and Froment [2]. On the other hand, the CDPM is based on simple single-pellet boundary conditions [15, 35], this therefore can not account for an existence of the solid-wall heat transfer. The CSPM generally considers the solid phase to be continuum [1, 4], as in Appendix. Intrapellet isothermality is often assumed in the calculation of effectiveness factor for the CSPM. For purposes of comparison with each model, the rate expression of the Eq. (12) is considered to be first order with respect to ethane during ethane hydrogenolysis, having the pre-exponential factor of 4.1×10^{17}. This assumption helps estimate an effectiveness factor for the system used. For computations, six collocation points in the axial, four in the external radial, and four in the pellet radial directions are used. The independence of the collocation point on the results has been checked using a refined point for some representative situations. The local temperatures obtained on the fined point differed less than 1% everywhere at the reactor center from those obtained on the standard point. The computing times were about 1 min for the CSPM, 18 min for the CDPM, and 23 min for the MDPM on the IBM/MVS main frame. The combined Eqs. (10a)-(10c) have required more computational effort and proven to be long to get the steady state profiles.

Fig. 1a shows the cross-sectional average temperatures as functions of axial position for the simulation conditions as given in Table 2. The cross-sectional average temperature is calculated using

$$\bar{T}_j=\int_A T_j(r)dA/\int_A dA=2\int_0^1 T_j(r)\ rdr. \tag{13}$$

A similar expression is used to compute the average concentra-

tion. The magnitudes of the cross-sectional average temperatures predicted by the CDPM is much higher than those of the MDPM near the hot spot position. There is less heat transfer through the reactor wall in the CDPM than the MDPM, even though the recommended effective lumped parameters [35] are used in the CDPM, causing relatively high fluid and solid temperatures. Although the average temperature is higher for the CDPM, the exit temperature is slightly lower. It is not too suprising that the MDPM predicts results similar to those calculated using the CSPM which involves convective and dispersion terms in the solid phase energy balance, as shown in Appendix. The computed differences between local solid and fluid temperatures are drastically greater for the CDPM than for either of the other models. Qualitative agreement between the predicted temperature from the MDPM and the experimental data [9] is observed. The hot spot occurs at 3 cm from the reactor inlet for the CDPM, and 3.6 cm for both the CSPM and the MDPM. Fig. 1b shows the cross-sectional average conversion profiles as functions of the axial position. The predicted conversion profile for the CSPM is much higher than that for the MDPM corresponding to the trend as the temperature. The radial temperature profiles at the hot spot are shown in Fig. 1c. At the center of the reactor diameter, the local solid temperature obtained from the CDPM is higher by approximately 30 degree than that obtained form the MDPM. The temperatures at the reactor center are much higher than those at the reactor wall.

Fig. 2a shows the time revolution of cross-sectional average solid temperature profiles predicted by the MDPM after a step change in feed temperature from 520 to 500 K. Immediately following the decrease in the inlet temperature, the transient maximum reactor temperature goes up. Such transient temperature rises, referred to as a "wrong-way" behavior, complicate reactor control schemes. This type of behavior has been noted [11, 14, 15, 44], and has been predicted theoretically [45, 46]. The cooler feed gas results in a gas stream with higher reactant concentration passing into the hot region of the catalyst bed, before it has a chance to heat the early part of the bed because the cool reactor wall remains unchanged and acts as a heat exchanger. A reduction in the feed gas temperature results in an increase of exit solid temperature as the hot spot travels downstream. As can be seen in Fig. 2b, the response of conversion profiles is a little slower than that of the temperature profiles. The difference in propagation speed of the temperature and concentration disturbances in the reactor causes the temperature to exhibit "wrong-way" behavior.

Fig. 3a and 3b show the transient responses of temperature and conversion predicted by the MDPM, respectively, for the operating conditions of 520 K inlet temperature and 1 atm reactor pressure. The rate expression of Eq. (12) is used in this computation. Notice that the conversion profiles change more rapidly than temperature profiles at the beginning of startup for $t = 0$. Thereafter the temperature changes much faster than conversion due to more heat produced in the catalyst. The highest temperature and conversion are observed at the steady state during the transient operation. The temperature difference between solid and fluid is much greater towards the entrance of the reactor throughout the whole operation. Fig. 3c shows the axial mean temperature as functions of the reactor length. The trend corresponds to Fig. 3a.

Sensitivities of the reactor responses have been studied with

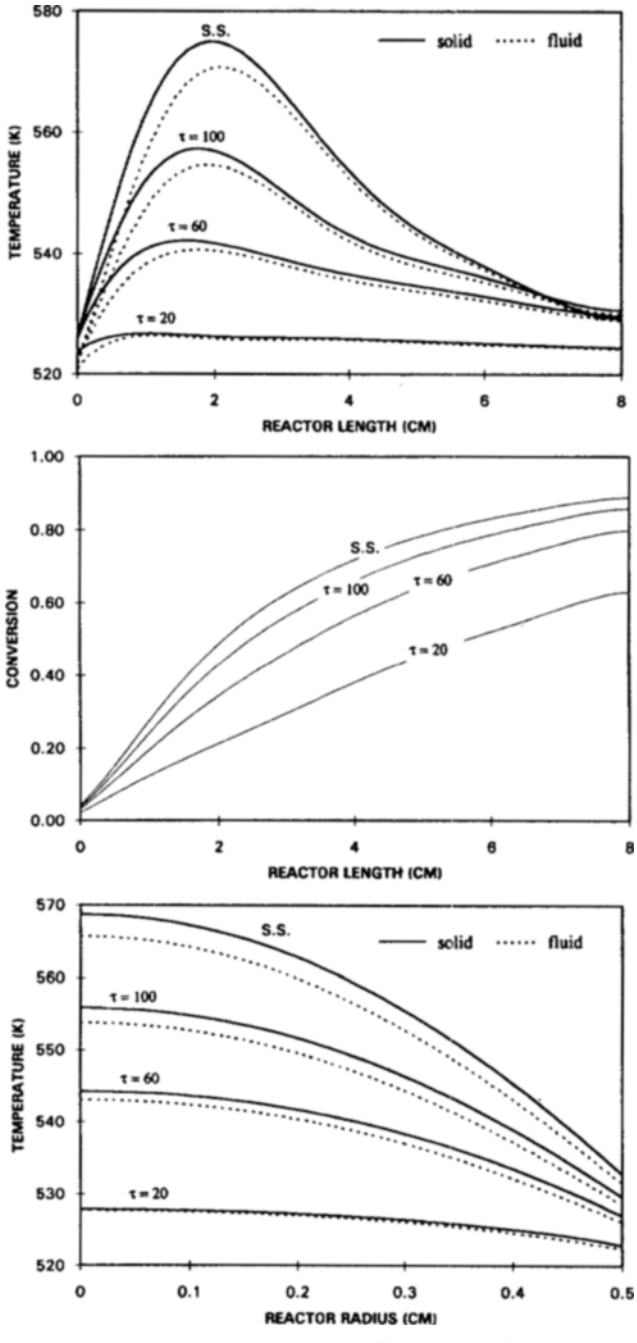

Fig. 3. Temperature and concentration profiles at unsteady state using the MDPM for the operating conditions of 520 K inlet temperature and 1 atm reactor pressure.

A. Cross-sectional average temperature profiles as functions of reactor length, B. Cross-sectional average conversion profiles as functions of reactor length, C. Axial mean temperature profiles as functions of reactor radius.

varying the transport parameter values by a factor of 20%, both higher and lower. For the MDPM, predictions of temperature and concentration profiles are relatively sensitive to the inlet fluid temperature, which is evident with the inclusion of axial dispersion in the boundary conditions at the entrance. On the other hand, the predictions are not too sensitive to the fluid axial thermal conductivity. In contrast, the radial fluid heat transfer and

interfacial heat transfer coefficients affect reactor behavior predictions drastically. These results agree with those of Odendaal et al. [5]. Predictions are more sensitive to the wall-solid heat transfer coefficient than the wall-fluid heat transfer coefficient. An apparent influence of intraparticle diffusivity effect on hot spot magnitude and position is observed. This influence depends on the particle size. A decrease in the particle size increase the maximum solid temperature rise in the bed. The reason is the fact of that a smaller particle reduces the intraparticle diffusional resistance, causing more heat of reaction. Complete conversion can be obtained by adjustment of pellet size. The use of radial velocity and porosity profiles affects the hot spot temperature and its position as well as exit conversion, as expected in low value of d_t/d_p. It increases the difference between fluid and solid temperatures at hot spot region.

CONCLUSIONS

It is common to apply simplifying assumptions for mathematical models of the packed bed reactor. The most general two dimensional heterogeneous model with modified single pellet boundary conditions has been discussed, avoiding some simplifying assumptions of earlier models. A detailed comparison is made between the different types of models. The MDPM is consistent with the CSPM under any given considerations. Since the CDPM does not present any programming advantage over the MDPM, moreover, the MDPM is of free calculation of effectiveness factor for any formidable reaction expression, it is preferable to use the MDPM for the simulation of the packed bed reactor. The magnitude and position of the hot spot in the reactor is different between the MDPM and the CDPM. Conduction in the solid is considered to be important in packed bed at low Reynolds number and should also be included for mathematical models.

The dynamic effects of the operating condition are examined. Undesirable wrong-way behavior in the transient maximum temperature has been observed for feed temperature decrease.

Parametric sensitivity is examined for several heat and mass parameters as well as for the effect of common simplifying hypotheses. Intraparticle effective diffusivity and particle size have been shown to be important for the hot spot magnitude and its position. The inclusion of radial velocity and porosity profile has been studied in this system.

ACKNOWLEDGMENTS

I am grateful for discussion and assistance of this study by T. S. Cale at Arizona State University, Tempe, Arizona, U. S. A.

APPENDIX : CONTINUUM SOLID PHASE MODEL EQUATIONS

Each phase for continuum solid phase model (CSPM) is treated as a continuum. The dimensionless form is:

For external fluid phase

Mass balance:

$$\frac{\partial c_f}{\partial \tau} = -\frac{\partial (uc_f)}{\partial z} + \frac{1}{Pe_{am}}\frac{\partial}{\partial z}\left(D_{ai}\frac{\partial c_f}{\partial z}\right) - \frac{1}{Pe_{rm}}\frac{1}{r}\frac{\partial}{\partial r}\left(D_{ri} r \frac{\partial c_f}{\partial r}\right) - \alpha_m (c_f - c_{sf}) \tag{A1}$$

Energy balance:

$$\frac{\partial T}{\partial \tau} = -u\frac{\partial T}{\partial z} + \frac{1}{Pe_{ah}}\frac{\partial}{\partial z}\left(k_{ai}\frac{\partial T}{\partial z}\right) + \frac{1}{Pe_{rh}}\frac{1}{r}\frac{\partial}{\partial r}\left(k_{ri} r \frac{\partial T}{\partial r}\right) - \alpha_h (T - T_s) \tag{A2}$$

at $\tau = 0$, $c_f = 1$, $T = 1$ (A3)

at $z = 0$, $\frac{\partial c_f}{\partial z} = \varepsilon_b\, Pe_{am}(c_f - 1)$, $\frac{\partial T}{\partial z} = \varepsilon_b\, Pe_{ah}(T - 1)$ (A4a)

at $z = 1$, $\frac{\partial c_f}{\partial z} = 0$, $\frac{\partial T}{\partial z} = 0$ (A4b)

at $r = 0$, $\frac{\partial c_f}{\partial r} = 0$, $\frac{\partial T}{\partial r} = 0$ (A5a)

at $r = 1$, $\frac{\partial c_f}{\partial r} = 0$, $\frac{\partial T}{\partial r} = Bi_{wf}(T_w - T)$. (A5b)

For the solid

Mass balance: $\frac{\partial c_{sf}}{\partial \tau} = \delta_1 (c_f - c_{sf}) - \delta_2 \eta \phi (c_s, T_s)$ (A6)

Energy balance:

$$\frac{\partial T_s}{\partial \tau} = \lambda_1 \frac{\partial}{\partial z}\left(k_{as}\frac{\partial T_s}{\partial z}\right) + \lambda_2 \frac{1}{r}\frac{\partial}{\partial r}\left(k_{rs} r \frac{\partial T}{\partial r}\right) + \lambda_3 (T - T_s) + \lambda_4 \eta \phi (c_s, T_s) \tag{A7}$$

at $\tau = 0$, $c_{sf} = 1$, $T_s = 1$ (A8)

at $z = 0$, $\frac{\partial T_s}{\partial z} = Pe_{ah}(T_s - 1)$ at $z = 1$, $\frac{\partial T_s}{\partial z} = 0$ (A9)

at $r = 0$, $\frac{\partial T_s}{\partial r} = 0$ at $r = 1$, $\frac{\partial T_s}{\partial r} = Bi_{ws}(T_w - T_s)$ (A10)

where effectiveness factor η is defined as:

$$\eta = \frac{1}{\varphi}\frac{3\varphi \coth(3\varphi) - 1}{3\varphi} \quad \text{with} \quad \varphi = \frac{R_p}{3}\sqrt{k_v/D_{em}}.$$

NOMENCLATURE

- a_v : catalyst interfacial surface area per catalyst volume
- A : matrix representing first derivative
- B : matrix representing Laplacian
- Bi_m : Biot number of pellet for mass ($k_g R_f/D_{em}$)
- Bi_h : Biot number of pellet for heat (hR_p/K_p)
- Bi_{wf} : fluid-wall Biot number ($h_{wf}R_t/K_f$)
- Bi_{ws} : solid-wall Biot number ($h_{ws}R_t/K_s$)
- c_v : heat capacity
- c : dimensionless concentration (C/C_o)
- C : concentration
- d : diameter
- D : dimensionless diffusivity of the fluid ($\mathcal{D}/\mathcal{D}_o$)
- $\mathcal{D}$: diffusivity in the fluid
- $\mathcal{D}_{em}$: effective diffusivity in the pellet
- h : interfacial heat transfer coefficient
- ΔH : heat of reaction
- k : dimensionless conductivity (K/K_o)
- K : conductivity
- k_g : interfacial mass transfer coefficient
- k_o : pre-exponential factor

L_t : reactor length
L : number of collocation point in the axial direction
M : number of collocation point in the radial direction
N : number of collocation point in the pellet radial direction
Pe_{am} : Peclet number for mass in the axial direction ($UL_t/\mathcal{D}_a\varepsilon_b$)
Pe_{rm} : Peclet number for mass in the radial direction ($UR_t^2/\mathcal{D}_rL_t\varepsilon_b$)
Pe_{ah} : Peclet number for heat in the axial direction ($UL_t\rho_fc_{vf}/K_{fa}\varepsilon_b$)
Pe_{rh} : Peclet number for heat in the radial direction ($UR_t^2\rho_fc_{vf}/K_{fr}L_t\varepsilon_b$)
Pe_{pm} : Peclet number for mass in the pellet ($UR_p^2/\mathcal{D}_{eff}L_t\varepsilon_p$)
Pe_{ph} : Peclet number for heat in the pellet ($UR_p^2\rho_pc_{vp}/K_pL_t$)
r : dimensionless radial coordinate in the bed ($\bar{r}/R_t$)
$\bar{r}$: radial coordinate in the bed
R : radius
$\Re$: reaction rate per catalyst volume
t : time
T : dimensionless temperature ($\bar{T}/\bar{T}_o$)
$\bar{T}$: temperature
u : dimensionless velocity (U/U_o)
U : superficial fluid velocity
W : weights
z : dimensionless axial coordinate ($\bar{z}/L_t$)
$\bar{z}$: axial coordinate in the bed

Greek Letters

α_h : defined in Eq. (2) $\{L_tha_v(1-\varepsilon_b)/U\rho_fc_{vf}\varepsilon_b\}$
α_m : defined in Eq. (1) $\{L_tk_ga_v(1-\varepsilon_b)/U\varepsilon_b\}$
β : defined in Eq. (10a) $\{R_pk_s/K_pa_vR_t^2(1-\varepsilon_b)\}$
β' : defined in Eq. (10a) $\{R_pk_s/K_pa_vL_t^2(1-\varepsilon_b)\}$
ε : voidage
δ_1 : defined in Eq. (A6) $(k_ga_vL_t/U)$
δ_2 : defined in Eq. (A6) (L_t/UC_{so})
ϕ : dimensionless reaction rate $\{\Re(C_p, \bar{T}_p)/\Re(C_o, \bar{T}_o)\}$
γ_h : defined in Eq. (7) $\{L_t(-\Delta H)/\bar{T}_o\rho_pc_{vp}U\varepsilon_p\}$
γ_m : defined in Eq. (6) $(L_t/C_oU\varepsilon_p)$
η : effectiveness factor
λ_1 : defined in Eq. (A7) $\{K_{sa}/L_tU\rho_sc_{vs}(1-\varepsilon_b)\}$
λ_2 : defined in Eq. (A7) $\{K_{sr}L_t/R_t^2U\rho_sc_{vs}(1-\varepsilon_b)\}$
λ_3 : defined in Eq. (A7) $(ha_vL_t/U\rho_sc_{vs})$
λ_4 : defined in Eq. (A7) $\{(-\Delta H)L_t/U\rho_sc_{vs}T_o\}$
ρ : density
τ : dimensionless time (U_t/L_t)
ξ : dimensionless radial coordinate in the pellet (x/R_p)

Superscripts and Subscripts

a : axial direction
b : bed
f : fluid
h : heat
i : species
j : index
k : index
l : index
m : mass
n : index
o : feed condition
p : pellet
r : radial direction
s : solid or surface
t : reactor tube
w : tube wall
z : axial position

REFERENCES

1. Froment, G. F.: in "Concepts and Design of Chemical Reactors", p. 179, eds. Whitaker, S. and Cassano, A. E., Gordon and Breach Sci. Publishers (1986).
2. DeWasch, A. P. and Froment, G. F.: *Chem. Eng. Sci.*, **26**, 629 (1971).
3. Pereira Duarte, S. I., Barreto, G. G. and Lemcoeff, N. O.: *Chem. Eng. Sci.*, **39**, 1017 (1984).
4. Khanna, R. and Seinfeld, J. H.: "Mathematical Modeling of Packed Bed Reactors: Numerical Solutions and Control Model Development", in Advances in Chemical Engineering, vol. 13, 1987.
5. Odendaal, W., Gobie, W. and Carberry, J.: *Chem. Eng. Comm.*, **58**, 37 (1987).
6. Schilson, R. E. and Amundson, N. R.: *Chem. Eng. Sci.*, **13**, 226 (1961).
7. Bischoff, K. B.: *Chem. Eng. Sci.*, **23**, 451 (1968).
8. Copelowitz, I. and Aris, R.: *Chem. Eng. Sci.*, **25**, 885 (1970).
9. Cale, T. S.: *J. Catal.*, **90**(1), 40 (1984).
10. Karanth, N. G. and Hughes, R.: *Chem. Eng. Sci.*, **29**, 197 (1974).
11. van Doesburg, H. and de Jong, W. A.: *Chem. Eng. Sci.*, **31**, 45 (1976).
12. Sharma, C. S. and Hughes, R.: *Chem. Eng. Sci.*, **34**, 613 (1979).
13. Puszynski, J., Snita, P., Hlavacek, V. and Hoffmann, H.: *Chem. Eng. Sci.*, **36**, 1605 (1981).
14. Windes, L. C., Schwedock, M. J. and Harmon Ray, W.: *Chem. Eng. Comm.*, **78**, 1 (1989).
15. Gatica, J. E., Romagnoli, J. A., Errazu, A. F. and Porras, J. A.: *Chem. Eng. Comm.*, **78**, 73 (1989).
16. Feick, J. and Quon, D.: *Can. J. Chem. Eng.*, **48**, 205 (1970).
17. Bilous, O. and Amundson, N. R.: *AIChE J.*, **2**, 117 (1956).
18. Danckwerts, P. V.: *Chem. Eng. Sci.*, **2**, 1 (1953).
19. Karanth, N. G. and Hughes, R.: *Cat. Rev. Sci. Eng.*, **9**, 169 (1974).
20. Lee, H. H.: "Heterogeneous Reactor Design", Butterworths Publishers, Boston, 1985.
21. Froment, G. F. and Bischoff, K. B.: "Chemical Reactor Analysis and Design", John Wiley & Sons, 1990.
22. Finlayson, B. A.: *Chem. Eng. Sci.*, **26**, 1081 (1971).
23. Young, L. C. and Finlayson, B. A.: *I&EC Fund.*, **12**, 412 (1973).
24. Finlayson, B. A.: *Cat. Rev. Sci. Eng.*, **10**, 69 (1974).
25. Villadsen, J. and Stewart, W. E.: *Chem. Eng. Sci.*, **22**, 1483 (1967).
26. Finlayson, B. A.: "Nonlinear Analysis in Chemical Engineering", McGraw-Hill Inc., 1980.
27. IMSL Math/Library, "Fortran Subroutines for Mathematical Applications", Version 1.0 IMSL, Houston, Texas, 1987.
28. Reid, R. C., Prausnitz, J. M. and Poling, B. E.: "The Properties of Gases and Liquids", McGraw-Hill, 1988.
29. Satterfield, C. N.: "Heterogeneous Catalysis in Practice", McGraw-Hill, 1980.
30. Ludlow, D. K.: Ph. D. Dissertation, Arizona State Univ., U. S. A., 1986.
31. Dixon, A. G. and Cresswell, D. L.: *AIChE J.*, **25**(4), 663 (1979).
32. Edwards, M. F. and Richardson, J. F.: *Chem. Eng. Sci.*, **23**, 109 (1968).
33. Fahien, R. A. and Smith, J. M.: *AIChE J.*, **1**, 28 (1955).

34. Dwivedi, P. N. and Upadhyay, S. N.: *Ind. Eng. Chem. Des. Dev.*, **16**, 157 (1977).
35. Wakao, N.: in "Recent Advances in the Engineering Analysis of Chemically Reacting Systems", ed. by Doraiswamy, L. K., John Wiley & Sons (1984).
36. Yagi, S. and Wakao, N.: *AIChE J.*, **5**, 79 (1959).
37. Olbrich, W. E.: "Chemica '70 Conference Proceedings", p. 101, Butterworths, London, England (1971).
38. Zehner, P. and Schlünder, E. U.: *Chem. Eng. Techn.*, **42**, 333 (1970); *ibid.*, **44**, 1303 (1972).
39. Gunn, D. J.: *Chem. Eng. Sci.*, **42**, 363 (1987).
40. Mehta, D. and Hawley, M. C.: *Ind. Eng. Chem. Proc. Des. Dev.*, **8**, 280 (1969).
41. Fahien, R. W. and Stankovic, I. M.: *Chem. Eng. Sci.*, **34**, 1350 (1979).
42. Dixon, A. G.: *Can J. Chem. Eng.*, **66**, 705 (1989).
43. Ahmed, M. and Fahien, R. W.: *Chem. Eng. Sci.*, **35**, 889 (1978).
44. Hoiberg, J. A., Lyche, B. C. and Foss, A. S.: *AIChE J.*, **17**, 1434 (1971).
45. McGreavy, C. and Naim, H. M.: *Can. J. Chem. Eng.*, **55**, 326 (1977).
46. Mehta, P. S., Sams, W. N. and Luss, D.: *AIChE J.*, **27**, 234 (1981).